Probing the Acyl-Binding Pocket of Aminoacylase-1[‡]

Holger A. Lindner,* Alain Alary, Marsha Wilke, and Traian Sulea*

Biotechnology Research Institute, National Research Council Canada, 6100 Royalmount Avenue, Montreal, Quebec, Canada H4P 2R2

Received October 26, 2007; Revised Manuscript Received January 9, 2008

ABSTRACT: The aminoacylase-1/metallopeptidase 20 (Acy1/M20) family features several L-aminoacylases useful in biocatalysis. Mammalian Acy1, in particular, has been applied in racemic resolution and reverse hydrolysis. Despite recent advances in our understanding of the active site architecture and functioning, determinants of Acy1 substrate specificity have remained uncharted. Comparison to bacterial homologues points to a sterically more restricted acyl-binding pocket for Acy1. Here we sought to map characteristics of the acyl-binding pocket of human and porcine Acy1. Toward this end, we determined Michaelis constants for an analogue series of aliphatic *N*-acyl-L-methionine substrates and translated the values into three-dimensional quantitative structure–activity relationship models employing the minimal topological difference-partial least square method. The QSAR models for the two enzymes suggest overall similar binding pockets in the acetyl-binding portion and indicate a general preference for straight-chain acyl moieties. Embedding of the QSAR map for human Acy1 in the structure of its metal-binding domain associates the side chain of Ile177 with limited acyl chain elongation which was not observed for the porcine enzyme. The topological model further supports roles of Thr347 and Leu372, which are both conserved in the porcine enzyme, in restricting acyl chain branching at the α- and β-positions, respectively. Mutational analyses confirmed our predictions for Thr347 and Leu372. Moreover, the T347S variant of human Acy1 exhibited markedly increased catalytic efficiency against *N*-benzoylamino acids, demonstrating the potential for engineering of substrate specificity in Acy1. We discuss the more general application of the employed procedure for protein design.

The aminoacylase-1/metallopeptidase 20 (Acy1/M20)[1] family from the MH clan is the largest sequence family of metallopeptidases (*1*). It can be divided into two functional subclasses, one of which features degradative dipeptidases and exopeptidases (EC 3.4), while the other comprises various amidohydrolases acting on carbon−nitrogen bonds other than peptide bonds (EC 3.5) (*2, 3*). Examples from the second subclass include bacterial (*4*) and plant (*5*) allantoate amidohydrolases (purine catabolism, EC 3.5.3.9), yeast βAS (β-alanine synthase, pyrimidine catabolism, EC 3.5.1.6) (*6*), bacterial succinyl-diaminopimelate desuccinylase (diaminopimelate/lysine biosynthesis, EC 3.5.1.18), and *N*α-acetyl-L-ornithine deacetylase (arginine biosynthesis, EC 3.5.1.16) (*7–9*). Additionally, the second subclass features bacterial L-carbamoylases (EC 3.5.1.87) (*10, 11*) and L-aminoacylases (EC 3.5.1.14) from bacterial (*12, 13*), archaeal (*14, 15*), and mammalian (Acy1) (*16–19*) sources. For archaea, mixed specificity aminoacylase/carboxypepti-

dase enzymes have also been described (*20, 21*). L-Carbamoylases (*10, 11*) and L-aminoacylases (*22–25*) have been applied in the production of enantiomerically pure L-amino acids through racemic resolution. L-Aminoacylases, including the mixed specificity enzymes, largely prefer substrates with uncharged L-amino acids and short-chain *N*-acyl moieties, mostly acetyl (*12–14, 20, 21, 26–28*). Porcine Acy1 (pAcy1) has also been applied in the synthesis of *N*-lauroyl-L-amino acids in a glycerol/water system (*29*).

Acy1, the founding member of the Acy1/M20 family (*30*), is ubiquitously expressed and functions in the salvage of Nα-acetylated amino acids from intracellular protein degradation (*31*). Recently, genetic Acy1 deficiency due to mutational enzyme inactivation was discovered as a novel inborn error of metabolism with yet unclear pathogenic significance (*32, 33*). For Acy1 of the rat intestinal mucosa, a protective role in degrading chemotactic N-formylated peptides of commensal bacteria has been demonstrated (*34*). Porcine Acy1 was shown to also hydrolyze *N*-benzoylamino acids, although with catalytic efficiencies (k_{cat}/K_M) at least 10-fold lower compared to those of the N-acetylated amino acids (*35*). On the other hand, the aminoacylase from *Thermococcus litoralis* favors *N*-benzoyl- over *N*-acetylamino acids (*15*), making it functionally more similar to *Campylobacter jejuni* hippurate hydrolase (EC 3.5.1.32) (*36*). Carboxypeptidase G2 (CPG2, EC 3.4.17.11) even acts on extended para-substituted *N*-benzoyl-L-glutamate derivatives and was originally discovered as a folate hydrolyzing enzyme (*37*). The enzyme is in use as a rescue agent (Voraxaze) for methotrexate (MTX)

* To whom correspondence should be addressed. H.A.L.: phone, (514) 496-1887; fax, (514) 496-5143; e-mail, Holger.Lindner@cnrc-nrc.gc.ca. T.S.: phone, (514) 496-1924; fax, (514) 496-5143; e-mail, Traian.Sulea@nrc-cnrc.gc.ca.

[1] Abbreviations: Acy1, aminoacylase-1; βAS, β-alanine synthase; CoMFA, comparative molecular field analysis; CPG2, carboxypeptidase G2 from *Pseudomonas* sp. strain RS-16; hAcy1, human Acy1; HPLC, high-performance liquid chromatography; MTD-PLS, minimal topological difference-partial least square; MTX, methotrexate; NAM, *N*α-acetyl-L-methionine; pAcy1, porcine Acy1; TFA, trifluoroacetic acid; 3D-QSAR, three-dimensional quantitative structure–activity relationship.

overdoses. Furthermore, its ability to release various mustard drugs from, among others, N-substituted *p*-aminobenzoyl-L-glutamic acid derivatives (*38*) makes CPG2 a candidate for enzyme prodrug therapy of solid cancers (*39, 40*).

Crystal structures for Acy1/M20 family enzymes feature two protein domains connected by flexible linkers (*4, 6, 41–46*).[2] The first domain is characteristic of the MH clan (*1*) and harbors a cocatalytic zinc center and an adjacent invariant glutamic acid residue that is thought to act as a general acid/base catalyst (*47, 48*). The second, smaller domain distinguishes the Acy1/M20 family. It is inserted in the middle of the Zn-binding domain and, with one exception, mediates enzyme dimerization. On the other hand, peptidase V (PepV, EC 3.4.13.3) exists as a monomer (*45*). The structure of its inserted domain mimics the arrangement of two associated dimerization domains (*49*). An inhibitor bound at the active site in the PepV crystal structure contacts active site residues from both enzyme domains which are seen locked in a closed conformation (*45*). While in most of the homodimer structures both enzyme domains in either subunit adopt an extended open conformation (*4, 6, 41–44*),[2] closed conformation-state structures with bound substrate or product were very recently reported also for dimeric βAS from *Saccharomyces kluyveri* (*46*). Molecular modeling supports formation of the catalytically competent active site through domain closure as well for CPG2 (*50*) and *Escherichia coli* allantoate amidohydrolase (*4*). In accordance with the closed conformation structures of PepV (*45*) and βAS (*46*), enzyme complementation assays with human Acy1 (hAcy1) have established that an invariant histidine (His206) and a highly conserved asparagine (Asn263) from the dimerization domain of the opposite subunit, as well as a moderately conserved arginine (Arg276) from the same subunit as the correlated zinc center, contribute to the active site (*49, 50*). Mutational analyses of βAS (*46*) and *Sinorhizobium meliloti* L-carbamoylase (*51*) are consistent with this scenario.

Despite these advances in the understanding of the catalytic machinery, interactions that determine substrate specificities in Acy1/M20 family enzymes are largely uncharacterized. The reduced specificity of Acy1 for *N*α-benzoyl- versus *N*α-acetyl-L-amino acids points to a more restricted acyl-binding pocket compared to that of *T. litoralis* aminoacylase, *C. jejuni* hippurate hydrolase, and certainly CPG2, enzymes that lack significant sequence identity to Acy1. Here we used steady-state kinetics, three-dimensional quantitative structure–activity relationship (3D-QSAR) analysis, and site-directed mutagenesis to characterize the acyl-binding pocket of human and porcine Acy1. Our results confirm the general preference of Acy1 for straight-chain acyl moieties and identify three amino acids in the metal-binding domain of hAcy1 predicted to restrict the binding of larger acyl groups. We could experimentally support this prediction for two of these residues, in the course of which we generated an hAcy1 variant with markedly increased catalytic efficiency versus *N*-benzoylamino acids. The more general application of the employed procedure is discussed.

Table 1: Forward Versions of Mutagenic Primers for hAcy1

mutant	oligonucleotide sequence[a]
I177G	5′-GCCCTGGATGAGGGC**GG**AGCCAATCCCACTGATGCC-3′
I177A	5′-GCCCTGGATGAGGGC**GC**AGCCAATCCCACTGATGCC-3′
I177V	5′-GCCCTGGATGAGGGC**G**TAGCCAATCCCACTGATGCC-3′
I177L	5′-GCCCTGGATGAGGGC**T**TAGCCAATCCCACTGATGCC-3′
T347S	5′-GATCATGCCTGCTGCCA**GT**GACAACCGCTATATC-3′
T347F	5′-GATCATGCCTGCTGCC**TTT**GACAACCGCTATATC-3′
L372G	5′-CCGCACACCTGTGCTG**GGG**CACGACCACGATGAACG-3′
L372A	5′-CCGCACACCTGTGCTG**GC**GCACGACCACGATGAACG-3′
L372V	5′-CCGCACACCTGTGCTG**GT**GCACGACCACGATGAACG-3′
L372I	5′-CCGCACACCTGTGCTG**AT**CCACGACCACGATGAACG-3′

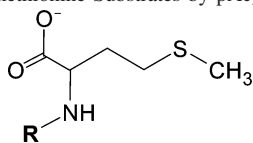*a* Altered nucleotides, which introduced the desired mutations, are underlined.

MATERIALS AND METHODS

Protein Expression and Characterization. Acy1 from human and hog and mutants of hAcy1 were expressed in a baculovirus expression vector system and purified as described previously (*26, 49*). Forward versions of the mutagenic primers are listed in Table 1. The sequences of the hAcy1 variants were confirmed by DNA sequencing. Protein concentrations were determined using the Bio-Rad (Hercules, CA) protein assay based on the original Bradford assay (*52*) with bovine serum albumin (Sigma, St. Louis, MO) as the standard. As a measure of enzyme stability, apparent "melting temperatures", T_m values, were determined as described previously (*53*). In brief, the purified enzyme in PCR tubes was overlaid with mineral oil, equilibrated at 25 °C, and slowly heated to 80 °C in an Eppendorf (Westbury, NY) Mastercycler PCR Thermocycler at a constant rate of 0.5 °C/min. Aliquots were withdrawn at 2 min intervals and subjected to determination of maximum activity. T_m values were read at the turning points of the S-shaped profiles. Protein oligomerization states were determined using analytical gel filtration as described previously (*50*).

Acylamino Acid Synthesis. All carboxylic acids used for synthesis, namely, propionic, butanoic, pentanoic, hexanoic, isobutanoic, isopentanoic, 2,2-dimethylpropionic, cyclopentanecarboxylic, and cyclohexanecarboxylic, were from Sigma and were of the highest purity available. *N*α-Acyl-L-amino acid derivatives were made by solid-phase synthesis on a Protein Technologies model PS3 automated peptide synthesizer (Protein Technologies, Inc., Tucson, AZ) using a standard *N*-α-(9-fluorenylmethyloxycarbonyl) procedure. Acylamino acid was cleaved from the resin using 92.5% (v/v) trifluoroacetic acid (TFA), 5% (v/v) water, and 2.5% (v/v) triisopropylsilane for 2 h with 10 mL/g of peptide resin. After evaporation under nitrogen, acylamino acid was dissolved in 50% (v/v) acetic acid, lyophilized, and purified by high-performance liquid chromatography (HPLC) using a Vydac C18 preparative column (22 mm × 250 mm) (Alltech, Guelph, ON) with a linear 2340 mL gradient from 0 to 40% (v/v) acetonitrile in 0.1% (v/v) TFA at a flow rate of 13 mL/min. Purity was evaluated by applying 50 μL of product to a Vydac C18 analytical column (4.6 mm × 250 mm) with a linear 40 mL gradient from 10 to 50% (v/v) acetonitrile in 0.1% (v/v) TFA at a flow rate of 1.0 mL/min. Elution profiles were monitored by absorbance at 220 nm for preparative HPLC and at 215 nm for analytical HPLC, where purities of final products were found to be ≥95%. Product masses were confirmed using a Sciex API III mass

Table 2: Kinetic Parameters for the Hydrolysis of *N*-Acyl-L-methionine Substrates by pAcy1 and hAcy1

R, acyl moiety	hAcy1			pAcy1		
	k_{cat} (s^{-1})	K_M (mM)	k_{cat}/K_M (M^{-1} s^{-1})	k_{cat} (s^{-1})	K_M (mM)	k_{cat}/K_M (M^{-1} s^{-1})
formyl	177	16.8	10500	200	35.4	5650
acetyl[a]	38.3	0.43	89100	134	2.72	49300
propionyl	25.7	0.34	75600	168	0.55	3054600
butanoyl	139	0.73	101500	107	0.31	345000
pentanoyl	16.2	0.19	85300	18.2	0.03	607000
hexanoyl	16.1	1.01	15900	4.3	0.01	430000
isobutanoyl	529×10^{-3}	15.3	35	89.8	58.5	1540
isopentanoyl	105×10^{-3}	4.27	25	694×10^{-3}	0.90	771
2,2-dimethylpropionyl[b]	$\sim 1.5 \times 10^{-3}$	168	$\sim 8.9 \times 10^{-3}$	$\sim 1.5 \times 10^{-3}$	585	$\sim 2.5 \times 10^{-3}$
cyclopentanoyl	13.3	7.18	1850	11.2	0.64	17500
cyclohexanoyl	6.23×10^{-3}	6.23	1	145×10^{-3}	0.31	468

[a] The data for hAcy1 with *N*-acetyl-L-methionine are identical to those reported in ref *49*. [b] The very low rates observed for hydrolysis of 2,2-dimethylpropionyl-L-methionine as a substrate by hAcy1 and pAcy1 complicated k_{cat} determination (see Experimental Procedures). Thus, only a limit value is given as an estimate of k_{cat}.

spectrometer (MDS Sciex, Concord, ON). Prior to injection, 5 µL of acetic acid was added to 50 µL of purified acylamino acid. Products were lyophilized and stored at 4 °C until they were used.

Acy1 Activity Assay. Acylamino acids used as substrates were synthesized as described above or were purchased from Bachem (King of Prussia, PA) [*N*α-acetyl-L-methionine (NAM), *N*α-formyl-L-methionine, *N*α-acetyl-L-glutamate, and *N*α-benzoyl-L-methionine] or Advanced ChemTech (Louisville, KY) (*N*α-benzoyl-L-glutamate). Acy1 amino acid deacylating activity was determined in quadruplicate at pH 7.4 via a discontinuous colorimetric assay with 2,4,6-trinitrobenzenesulfonic acid on 96-well microtiter plates as described previously (*26*). Care was taken to develop the assay during the linear phase of the primary reaction. Plates were sealed with incubations of more than 1 h. With one exception (see below), not more than 16 h was necessary. Controls were carried out showing that substrates were stable and that enzymes did not lose activity under the reaction conditions over the incubation period. Exceptionally, the extremely low rates observed with 2,2-dimethylpropionyl-L-methionine as a substrate (Table 2) necessitated reaction times of up to 120 h. However, enzymatic activity over this long time period could not be reproducibly retained in independent measurements. We did, therefore, not attempt to derive definite values for the catalytic constant, k_{cat}, from these measurements, and the values preceded by the tilde (∼) in Table 2 represent approximations. Determination of the Michaelis–Menten constant, K_M, was however less affected. Steady-state kinetics were evaluated by nonlinear regression analysis with SigmaPlot (Systat Software Inc., San Jose, CA), using the Michaelis–Menten equation [$v = (V_{max}[S])/(K_M[S])$], where K_M represents the substrate concentration at half-saturation. The k_{cat} value was calculated using the equation $V_{max} = k_{cat}[E]$, where [E] represents the total enzyme concentration. In situations where the rate versus substrate concentration plots showed no curvature, i.e., measurements were obviously performed far below K_M, the k_{cat}/K_M values were obtained by dividing the slopes by the enzyme concentrations (cf. Tables 3 and 5). All parameters reported exhibited errors of <20%.

3D-QSAR. The minimal topological difference-partial least square (MTD-PLS) method (*54–56*) was used to derive 3D-QSAR models for hAcy1 and pAcy1 that relate the experimentally determined linearized K_M values, which are indicative substrate binding affinities, to topological (steric) representations of the corresponding substrate analogues. To eliminate electrostatic effects, only the data for the 11 *N*-acyl-L-methionine substrates with aliphatic acyl substituents were included (Table 2). The 3D structures of these 11 substrate analogues were built as tetrahedral intermediates formed by the attack of a dinuclear Zn-activated water nucleophile on the acyl carbonyl carbon atom, using CONCORD (*57*) in Sybyl 6.9 (Tripos, Inc., St. Louis, MO). An initial structural alignment of the variable portions of the substrates, i.e., the acyl moieties, was generated by fitting over a constant region adjacent to the acyl group, i.e., the reactive tetrahedral center and its first-shell substituents, $-C(O^-)(OH)(NH-)$. This structural alignment was then translated into a hypermolecule consisting of 10 vertices that approximate the relative 3D positioning of all non-hydrogen atoms of the superimposed analogues.

Two alignment rules were applied to generate the specific 3D geometry of the hypermolecule shown in Figure 1 (schematized in the Supporting Information): (1) the MTD formalism (*58–63*) that implies a maximal steric overlap (i.e., the minimal topological difference) between analogues and (2) the preferred all-trans conformations for flexible moieties, extending from the nitrogen atom of the scissile amide bond up to the farthest terminal atom of an aliphatic acyl chain. These rules were straightforwardly applied to build a unique 3D hypermolecule by aligning the short groups formyl and acetyl, the 3-fold symmetrical dimethylpropionyl moiety, the linear propionyl, butanoyl, pentanoyl, and hexanoyl moieties, and the branched isobutanoyl moiety. The three remaining, branched, moieties [isopentanoyl, cyclopentanoyl, and cyclohexanoyl (in the preferred chair conformation)] could each be added to the aligned set of analogues in two favorable conformational states, while complying with the two alignment rules set above. This can formally lead to distinct 3D geometries in the regions of the hypermolecule occupied by these analogues (vertices 7, 9, and 10; see the Supporting

Table 3: Stability Features of hAcy1 Mutants and Kinetic Parameters for the Hydrolysis of NAM and Selected *N*-Acyl-L-methionine Probe Substrates

	apparent molecular mass (kDa)[a]	T_m (°C)	acyl moiety	k_{cat} (s^{-1})	K_M (mM)	K_M (fold change relative to that of the wild type)	k_{cat}/K_M (M^{-1} s^{-1})
wild type	99	64[b]	c				
I177A	90 (15%)	54	acetyl	66.7	1.14	2.7 ↑	58500
	39 (85%)		hexanoyl	9.51	3.56	3.5 ↑	2670
I177L	97	66	acetyl	93.7	1.72	4 ↑	54500
			hexanoyl	39.4	5.22	5.2 ↑	7550
T347G	97	57[b]	acetyl[d]	46.0	2.78	6.5 ↑	16600
			cyclohexanoyl[e]	NM[f]	NM[f]		4.01
T347S	95	65	acetyl	64.6	0.40	1.1 ↓	162000
			cyclohexanoyl	129×10^{-3}	1.17	5.3 ↓	110
T347F	49	52	acetyl	1.2	0.76	1.8 ↑	1580
L372G	96	68	acetyl	16.6	4.32	10 ↑	3840
			isopentanoyl[e]	NM[f]	NM[f]		137
L372A	97	70	acetyl[e]	NM[f]	NM[f]		2360
			isopentanoyl	5.36	2.1	2.0 ↓	2550
L372V	409 (15%)	60	acetyl	12.1	2.76	6.4 ↑	4380
	96 (85%)		isopentanoyl	0.34	0.54	7.9 ↓	630
L372I	90 (84%)	59	acetyl	4.49	1.35	3.1 ↑	3330
	16 (16%)		isopentanoyl	2.01	7.29	1.7 ↑	276

[a] In cases where more than one species was detected, the respective percentage from the total protein is given in parentheses. [b] The T_m values for the wild type and the T347G mutant are identical to those reported in ref 49. [c] See Table 2 for the kinetic parameters of the wild-type enzyme. [d] The kinetic data with *N*-acetyl-L-methionine for the T347G mutant are identical to those reported in ref 49. [e] The kinetics for T347G, L372A, and L372G with *N*-cyclohexanoyl-L-methionine, *N*-acetyl-L-methionine, and *N*-isopentanoyl-L-methionine, respectively, were linear with up to 20 mM substrate. [f] Not measurable.

Table 4: Statistical Parameters of the MTD-PLS Models for Binding of *N*-Acyl-L-methionine Substrates with Aliphatic Acyl Groups by hAcy1 and pAcy1[a]

QSAR model ($N = 11$; PC = 5)	R^2 (SEE)	F	Q^2 (SEP)	C
hAcy1, log K_M (M)	0.997 (0.066)	365.664	0.200 (1.131)	−1.751
pAcy1, log K_M (M)	0.993 (0.170)	135.550	0.729 (1.032)	−1.391

[a] N is the number of analogues. PC is the number of principal components. R^2 is the squared correlation coefficient. SEE is the standard error of estimates. F is the Fisher coefficient. Q^2 is the leave-one-out cross-validation correlation coefficient. SEP is the leave-one-out cross-validation standard error of predictions. C is the constant term in the final QSAR regression model, which corresponds to the unoccupied hypermolecule and should reflect the log K_M value of the *N*-formyl-L-methionine substrate.

Information); albeit, these alternate geometries correspond to statistically equivalent QSAR models. The 3D geometry selected in these regions of the hypermolecule (Figure 1) appears to be the one better accommodated into the putative acyl-binding pocket of the hAcy1 (see below).

The MTD hypermolecule occupancy vectors for each acyl group (given as Supporting Information) represented the steric descriptor used as the independent variable in the QSAR regression against the experimental log(K_M) data. The implementation of the PLS regression (64–66) in Sybyl 6.9 was used to generate the leave-one-out cross-validated and final QSAR models. A graphical spatial display of the MTD-PLS 3D-QSAR model was obtained by mapping the resulting signed regression coefficients onto the corresponding vertices of the hypermolecule, thus indicating atom/group contributions to substrate binding affinity. The hypermolecule with assigned 3D-QSAR coefficients was embedded in a putative S1 (i.e., acyl-binding) subsite of hAcy1 in two steps. (i) The hypermolecule was superimposed onto the tetrahedral intermediate modeled previously (50) in complex with the closed form of the CPG2, an enzyme homologous to Acy1, by fitting of the heavy atoms forming the tetrahedral reactive center −C(O$^-$)(OH)(NH−), and (ii) structural superposition of the CPG2 model onto the partial crystal structure of hAcy1 (consisting of only the Zn-binding domain of the T347G

mutant; Protein Data Bank entry 1Q7L) (49) was carried out by fitting of the dinuclear Zn centers and their coordination sphere atoms.

RESULTS

Steady-State Kinetics for hAcy1 and pAcy1 with N-Acyl-L-methionine Substrates. We sought to map out the shape of the acyl-binding pocket of Acy1 by a 3D-QSAR approach. To this end, we designed a series of 11 *N*-acyl-L-methionine substrates, in which the acyl moiety was systematically modified, and determined steady-state kinetic parameters for their hydrolysis by both the human and porcine enzymes. These modifications of the acyl moiety were limited to saturated aliphatic groups to separate steric effects from electrostatic contributions. Specifically, these modifications resulted in the following acyl substituents (Table 2): formyl, acetyl, propionyl, butanoyl, pentanoyl, hexanoyl, isobutanoyl, isopentanoyl, 2,2-dimethylpropionyl, cyclopentanoyl, and cyclohexanoyl.

Table 2 summarizes the determined kinetic parameters. Straight-chain extension of the formyl up to the hexanoyl substituent decreased the K_M values of 16.8 mM for hAcy1 and 35.4 mM for pAcy1 to the micromolar range. This accounted for up to almost 10-fold enhancements of catalytic efficiencies for hAcy1 and an enhancement of 2 orders of magnitude for pAcy1. For both enzymes, introduction of the dimethylpropionyl moiety resulted in the lowest k_{cat} and the highest K_M values measured, leading to approximately 10^6-fold reductions in k_{cat}/K_M compared to those of the formyl moiety. Human Acy1 also exhibited considerably lower catalytic efficiencies with the other two branched-chain acyl substituents, namely, 300-fold for isobutanoyl and 420-fold for isopentanoyl, mainly due to reduced k_{cat} values. The corresponding k_{cat}/K_M values for pAcy1 were decreased little to moderately, i.e., 3.7- and 7.3-fold, as both parameters changed either only slightly (isobutanoyl) or in the same direction (isopentanoyl). Porcine Acy1 exhibited a 12-fold, and hAcy1 even a 10.5×10^3-fold, lower catalytic efficiency

Table 5: Kinetic Parameters for the Hydrolysis of *N*-Benzoyl- and *N*-Acetyl-L-methionine and -L-glutamate Substrates by Wild-Type Porcine and Human Acy1 and the T347S Mutant of hAcy1

acy1 enzyme	acyl moiety	amino acid moiety	k_{cat} (s^{-1})	K_M (mM)	k_{cat}/K_M (M^{-1} s^{-1})
pAcy1	acetyl	Met[a]	134	2.72	49300
		Glu	207	102	2030
	benzoyl	Met	1.3	0.38	3420
		Glu	115×10^{-3}	3.71	31
hAcy1	acetyl	Met[a]	38.3	0.43	89100
		Glu	156	63	2480
	benzoyl	Met	158×10^{-3}	0.81	198
		Glu	10.1×10^{-3}	1.63	6.2
hAcy1 T347S	acetyl	Met[b]	64.6	0.40	162000
		Glu	63.4	70	906
	benzoyl	Met	20.1	0.41	49000
		Glu	NM[c]	NM[c]	1020

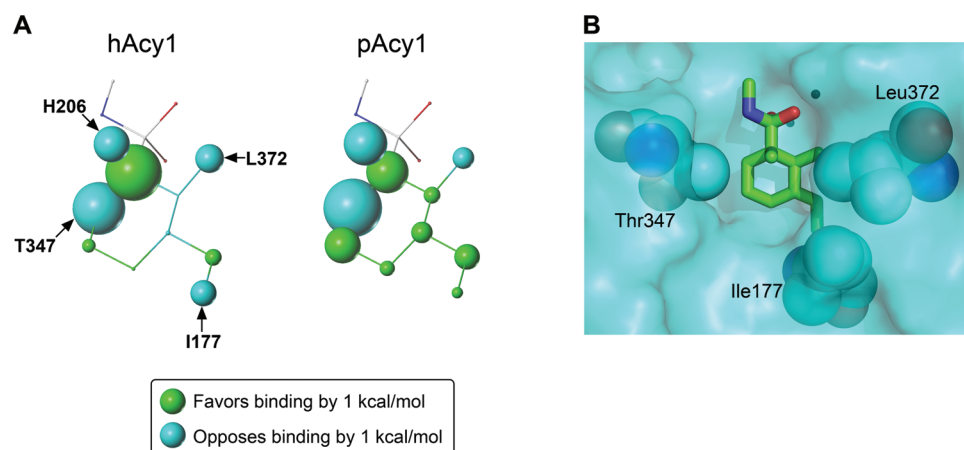[a] Values taken from Table 2. [b] Values taken from Table 3. [c] Not measurable.

FIGURE 1: Steric mapping of the aminoacylase acyl-binding site. (A) Graphic representation of the MTD-PLS 3D-QSAR models for binding of *N*-acyl-L-methionine substrates with aliphatic acyl groups in the S1 subsites of hAcy1 and pAcy1. Signed regression coefficients at the atom/group position of the aligned set of acyl groups are mapped onto the corresponding vertices of the hypermolecule. The resulting atom/group steric contributions to substrate binding affinity, converted into kilocalories per mole, are represented by spheres color-coded in green (favorable contributions) and cyan (unfavorable contributions), with radii scaled by the magnitude of the contributions (see the legend). In the left panel, representing the 3D-QSAR model for the S1 pocket of hAcy1 whose partial crystal structure has been determined (*49*), the arrows assign specific protein residues which may restrict the size of the pocket (see panel B) to substrate locations with detrimental binding contributions. (B) Embedding of the topological hypermolecule representing the aligned set of investigated aliphatic acyl groups into the hAcy1 structure. The hypermolecule is shown as sticks; the crystal structure of the T347G mutant of the hAcy1 metal-binding domain (*49*) is shown with a translucent cyan surface, and residues Ile177 and Leu372 are shown as CPK models. Residue Thr347 (CPK model), seen here to penetrate above the molecular surface, is inferred from the corresponding residue of CPG2 (Thr361), using a previously developed substrate-bound closed-state model of CPG2 (*50*) aligned onto the hAcy1 structure as described in Materials and Methods. The hAcy1 residue His206 from the dimerization domain, which was mutagenized in our previous work (*50*) and whose position can also be inferred from the aforementioned CPG2 model, has been omitted for clarity. Panel B was created with PyMOL 0.99rev8 (DeLano Scientific, San Carlos, CA).

with the cyclohexanoyl moiety, compared to the formyl moiety. Nevertheless, pAcy1 displayed higher binding affinities, as judged by K_M values, for the substrate with the cyclohexanoyl moiety (114-fold) and with the cyclopentanoyl moiety (55-fold) than for that with formyl-L-methionine.

3D-QSAR. To map the steric requirements of the acyl-binding pocket of Acy1, the binding affinity data expressed by the K_M values measured in this work for the aliphatic series of *N*-acyl-L-methionine substrates against the human and porcine enzymes were translated into 3D-QSAR models. To this end, we employed the MTD-PLS method (*54–56*), which uses PLS regression (*64–66*) to relate the biological activity to a hypermolecular structural description of the congeneric series of ligands spatially aligned within the MTD paradigm (*58–63*). As seen from Table 4, the MTD-PLS QSAR models derived at five principal components explain well the variance in the linearized K_M values within this series of aliphatic acyl substrates binding to either human or porcine Acy1. Leave-one-out cross-validation results indicate an

increased robustness of the model derived for the porcine enzyme compared to that for the human enzyme.

The associated MTD-PLS maps (Figure 1A), consisting of regression coefficients at the hypermolecule vertices, indicate that a cavity suitable for accommodating only one carbon atom connected to the attacked carbonyl (i.e., the acetyl group) is well-shaped (beneficial binding contribution in the QSAR maps). Furthermore, this acetyl-binding cavity is partially surrounded by stiff walls (detrimental binding contributions for multiple substitutions of the acetyl methyl group). Farther from the reaction center, the S1 pocket of pAcy1 is predicted to be more spacious (and less fragmented) than in the human enzyme.

We embedded the 3D hypermolecule with the associated MTD-PLS map into the available partial crystal structure of hAcy1 (*49*) superimposed onto the model of substrate-bound CPG2 in the closed conformation (*50*) (Figure 1B). This provides some level of structural rationalization in terms of residues that may form the walls of the S1 subsite as reflected

by detrimental steric contributions in the QSAR map of the human enzyme (arrows in Figure 1A). Specifically, the side chains of Thr347 from the Zn-binding domain of one subunit and His206 from the dimerization domain of another subunit in a dimeric hAcy1 are likely candidates responsible for severely restricting the space needed for α-branching of the acyl group [e.g., K_M(dimethylpropionyl) > K_M(isobutanoyl) ≫ K_M(propionyl) for both hAcy1 and pAcy1]. Both residues are conserved in the porcine enzyme. Restriction of β-branching of the acyl group (e.g., isopentanoyl) appears in the QSAR maps of both enzymes, is less pronounced than restriction of α-branching, and is associated with the side chain of Leu372 in hAcy1 (conserved in pAcy1). A steric repulsion in a region remote from the catalytic center is also present but only in the QSAR map of hAcy1. This region, which would need to be accessed to accommodate the terminal methyl group of the hexanoyl moiety, may be restricted by residue Ile177 of hAcy1 (leucine in pAcy1).

Characterization of hAcy1 Mutants. Our 3D-QSAR analysis (Figure 1) predicts that the side chains of Ile177, His206, Thr347, and Leu372 contribute to the walls of the acyl-binding pocket of hAcy1. We hypothesized that side-chain size reduction or different side-chain branching, introduced by site-directed mutagenesis at any of these positions, could generate a spatially less restricted acyl-binding pocket. We further assumed that such mutants of hAcy1 might exhibit improved binding and catalytic efficiencies toward substrate analogues (probe substrates) requiring access to the freed locations in the acyl-binding pocket. However, we did not pursue mutagenesis at position 206, since this histidine was shown to be implicated directly in the catalysis (*49, 50*). We constructed glycine, alanine, valine, and leucine mutants of Ile177, predicted to restrict side-chain elongation beyond the δ-position. No protein expression could be detected for the I177G variant. For the I177V mutant, a major band with an apparent molecular mass of 35 kDa, instead of the expected value of 46 kDa (*26*), was visible via SDS−PAGE already in the whole cell extract of the expression culture, indicating sensitivity of this protein to proteolysis. This precluded further analysis of the glycine and valine mutants of Ile177, and only I177A and I177L were analyzed further. In addition to our previously described glycine mutant of Thr347 (*49*), we mutated this residue that we predicted to restrict α-branching to serine and also to a bulkier residue, phenylalanine. Furthermore, we replaced Leu372 that we predicted to restrict β-branching with a glycine, alanine, valine, or isoleucine residue.

Like the T347G mutant (*49*), I177A, I177L, T347S, T347F, L372G, L372A, L372V, and L372I exhibited the same expression and purification behavior as the wild-type enzyme and appeared homogeneous as assessed by SDS−PAGE (not shown). Determination of apparent molecular masses by analytical gel filtration (Table 3) suggested the presence of a protein dimer (92 kDa, calculated) as the only detectable species for the wild type and the I177L, T347G, T347S, L372G, and L372A variants. Besides the putative dimer, one additional species, accounting for 15% of the total protein, was visible with the valine and the isoleucine mutants of Leu372. For L372V it likely represented a protein tetramer and for L372I a degradation product that was not detected via SDS−PAGE. In both cases, this was associated with slightly reduced T_m values, whereas mutation of Leu372 to

glycine or alanine entailed somewhat increased thermal stabilities (Table 3). The two remaining mutants, I177A and T347F, exhibited impaired and no detectable dimer formation, respectively. Only 15% of the I177A protein behaved as a dimer, while the rest eluted as a potential monomer. Only monomer was detected for T347F. For the I177A and T347F variants, T_m was reduced by 10 and 12 °C, respectively. Among the fully dimeric variants, only T347G exhibited a notably reduced T_m (by 7 °C).

Kinetics of hAcy1 Mutants. First, we assessed the performance of our hAcy1 mutants with NAM as a substrate (Table 3). The catalytic efficiency of T347F was reduced 56-fold relative to that of wild-type hAcy1, without a notable reduction in K_M. Catalytic efficiencies for T347S, I177A, and I177L were changed less than 2-fold, and T347G exhibited a moderate 5.4-fold reduction in k_{cat}/K_M. Altering Leu372, however, reduced k_{cat}/K_M at least 20-fold for all four mutants, L372G, L372A, L372V, and L372I. Most mutants exhibited low to moderate increases in K_M for NAM. Noteworthy are the facts that mutation of Leu372 to glycine increased K_M 10-fold, L372A could not be saturated, and thus K_M could not be measured.

We next determined kinetics using appropriate probe substrates to test our predictions derived from the binding site-embedded QSAR map of hAcy1 (cf. Figure 1A, left panel, and Figure 1B). The Ile177, Thr347 (except for T347F), and Leu372 mutants were tested in combination with *N*α-hexanoyl-L-methionine, *N*α-cyclohexanoyl-L-methionine, and *N*α-isopentanoyl-L-methionine, respectively (Table 3). Compared to wild-type hAcy1 (Table 2), I177A and I177L exhibited 6- and 1.9-fold reduced k_{cat}/K_M values, respectively, with *N*α-hexanoyl-L-methionine. Measured with *N*α-cyclohexanoyl-L-methionine, k_{cat}/K_M was increased 4-fold for T347G and 110-fold for T347S, and measured with *N*α-isopentanoyl-L-methionine, k_{cat}/K_M was increased 5.5-fold for L372G, 25-fold for L372V, 11-fold for L372I, and 102-fold for L372A. In three of these cases, we observed reductions in K_M, namely, 7.9-fold for L372V, 5.3-fold for T347S, and 2-fold for L372A. The K_M values for T347G with *N*α-cyclohexanoyl-L-methionine and for L372G with *N*α-isopentanoyl-L-methionine were immeasurable due to a lack of saturation. For the remaining mutants, we observed low to moderate increases in K_M.

We further compared the performances of wild-type porcine and human Acy1 and the T347S variant of hAcy1 against those of the *N*-acetyl and *N*-benzoyl derivatives of L-methionine and L-glutamate (Table 5). We found that pAcy1 displays 14- and 66-fold lower catalytic efficiencies against the *N*-benzoyl versus *N*-acetyl derivatives of methionine and glutamate, respectively. These differences are even more pronounced for hAcy1, i.e., 450- and 400-fold, respectively. The Thr-to-Ser mutation at position 347 in hAcy1 increased k_{cat}/K_M against benzoylmethionine and benzoylglutamate 248- and 165-fold, respectively, without significantly affecting hydrolysis of the corresponding *N*-acetylamino acid derivatives.

DISCUSSION

Aminoacylase enzymes from the Acy1/M20 family, including Acy1 from porcine kidney, have found various applications in biocatalysis (*22–25, 29*). Recent studies on

hAcy1 (*49, 50*) have advanced our understanding of the active site architecture and catalytic functioning of this group of enzymes. The determinants of aminoacylase substrate specificity that establish enzyme utility, however, have so far remained uncharted. Here we sought to map the characteristics of the acyl-binding pocket of human and porcine Acy1. To this end, we measured steady-state kinetics for an analogue series of aliphatic *N*-acyl-L-methionine substrates and translated the obtained K_M values into 3D-QSAR models employing the MTD-PLS method. Like the more popular comparative molecular field analysis (CoMFA) method (*67*), the MTD-PLS method can also produce a straightforward graphical translation of the regression model into a negative image of the binding site architecture. However, compared with CoMFA, MTD-PLS has some appeal since structural descriptors are assigned directly to atomic positions in the hypermolecule (cf. Figure 1A) rather than onto a sparse rectangular grid embedding the aligned set of ligands.

Ligand alignment based 3D-QSAR methods like MTD-PLS and CoMFA are not docking methods: the step of embedding the resulting 3D map of binding contributions into the corresponding putative binding site is accomplished externally either by structural comparisons with analogues cocrystallized or modeled in complex with the target protein or, in the absence of such data, by computational docking methods. On the basis of the currently available plethora of docking-scoring functions coupled with pose and conformational sampling strategies, there is a growing consensus indicating that correct docking of ligands to their cognate binding sites is a more tractable problem than accurate scoring of ligand binding affinities (*68–70*). Given this challenge of current computational scoring methods, we believe that for binding site profiling at the protein surface, empirical, QSAR methods capable of generating 3D maps of binding contributions are generally advantageous over computational scoring methods. This stems primarily from a higher accuracy in the quantification of binding affinities in the case of QSAR models based on experimental measurements, in comparison with computational affinity ranking of ligand analogues based on still maturing scoring functions (*71–74*). Also, atomic-level profiling of binding affinity contributions is straightforwardly encoded in the 3D maps from QSAR methods like MTD-PLS and CoMFA. In contrast, atomic decomposition schemes based on computationally scored binding affinities are rarely accessible, not always easily interpretable (*75, 76*), and inherit the approximations of the underlying scoring function (*77, 78*).

The leave-one-out cross-validation results for our MTD-PLS QSAR models (Table 4) indicate a better reliability for the model derived for the porcine enzyme than of that for the human enzyme. However, cross-validation results have to be treated with caution in this series, since exclusion of certain analogues (dimethylpropionyl, isopentanoyl, hexanoyl, and cyclohexanoyl) effectively drops certain hypermolecular vertices (descriptors) from the models generated during cross-validation, hence leading to uncertainties in predicting the biological activity for the excluded analogues (lower Q^2 values).

Our MTD-PLS QSAR models for hAcy1 and pAcy1 show that the acyl-binding pockets of these enzymes are overall similar (Figure 1A), which is not surprising given the high degree of conservation in the putative S1-defining sequence

(*50*). Steric interaction with the carbon atom directly adjacent to the electrophilic reaction center appears to contribute most significantly to binding. Both enzymes generally prefer straight-chain acyl moieties, while branching at the α- and β-positions, respectively, is restricted. In fact, occupancy at each of the vertices representing a linear acyl chain up to the ε-position appears to invariably favor binding to pAcy1, whereas occupancy at the ε-position opposes binding to hAcy1. We assume that these interactions are important for the ability of pAcy1 to function in the synthesis of *N*-lauroyl-L-amino acids via reverse hydrolysis (*29*).

Embedding of the MTD 3D hypermolecule in the structure of the metal-binding domain of hAcy1 (Figure 1A, left panel, and Figure 1B) predicts that Ile177 sterically interferes with accommodation of the terminal methyl group of the hexanoyl moiety. However, this prediction could not be supported by the kinetic analysis of the obtained alanine and leucine mutants as parameters for both I177A and Ile177L were changed only slightly (Table 3). If any, there was a marginal increase in K_M with both NAM and *N*α-hexanoyl-L-methionine. Notably, the lack of expression for I177G, partial degradation of I177V, and impaired dimerization as well as thermal stability for I177A (Table 3) indicate a structural role for Ile177, complicating its mutational analysis.

The topological model of the aligned probe substrates (Figure 1A, left panel, and Figure 1B) further suggests that the side chains of Thr347 and, additionally, the dimerization domain residue His206 that is inserted into the active site through domain closure (*4, 6, 45, 46, 49–51*) both sterically restrict α-branching of the acyl moiety. Given the catalytic role of His206 (*49, 50*), we focused on Thr347. Mutation of this residue to phenylalanine (T347F), to further occlude the S1 pocket, thermally destabilized and largely dissociated the enzyme dimer (Table 3), suggesting a major impact on conformational integrity. We thus excluded the T347F mutant from the analysis with the probe substrate. Complete side-chain removal (T347G) also thermally destabilized the enzyme and led to reduced substrate affinities. The minimal structural change, however, introduced by the Thr-to-Ser mutation (T347S) did not alter enzyme stability. The observed 5.3-fold reduction in K_M for T347S measured with the probe substrate *N*α-cyclohexanoyl-L-methionine (Table 3) thus argues in favor of the predicted contribution of Thr347 to the formation of the proximal region of the acyl-binding pocket and putatively involves its γ-methyl group.

Moreover, the model (Figure 1A, left panel, and Figure 1B) identifies Leu372 as a likely source of restricted β-branching. Mutation of this residue to glycine, isoleucine, valine, or alanine enhanced the catalytic efficiency 11−102-fold against the probe substrate, *N*α-isopentanoyl-L-methionine (Table 3). Most notably, the L372V mutant exhibited enhanced binding affinity for *N*α-isopentanoyl-L-methionine as judged by a 7.9-fold reduced K_M value. We interpret this result as support for our prediction that Leu372 directly contributes to the walls of the acyl-binding pocket approaching the β-position of the acyl chain in the Michaelis complex. The negative impact (6.4-fold) of the L372V mutation on the K_M measured with NAM is not totally unexpected, as it may be explained by the mutant enzyme displaying a larger acyl-binding pocket that is suboptimal for accommodation of the methyl group of the small acetyl substituent. That is, relative to the leucine side chain in the wild-type enzyme,

the shorter valine side chain would establish weaker van der Waals interactions with the NAM methyl group. A similar phenomenon may explain the reduced affinities observed with the glycine and alanine mutants of Leu372 (Table 3).

Unlike some of its bacterial homologues (*15, 36, 37*), pAcy1 reportedly exhibits a lower efficiency in the hydrolysis of $N\alpha$-benzoyl-L-amino acid versus $N\alpha$-acetyl-L-amino acid substrates (*35*) which was an original indication for a more restricted acyl-binding pocket in the mammalian enzyme. Using the corresponding methionine and glutamate derivatives for comparison, we found that this applies all the more to hAcy1 (Table 5). Mutation of Thr347 in hAcy1 to Ser not only preserved the enzyme's deacetylating activity but also enhanced its catalytic efficiency against the *N*-benzoyl derivatives by 2 orders of magnitude (Table 5). This mutation thus appears not only to open the proximal acyl-binding pocket but also to improve the fit for the bulky benzoyl substituent during catalysis.

The procedure employed here to delineate the shape of the Acy1 acyl-binding pocket has led to mutant enzymes with improved catalytic efficiencies toward specific substrate analogues, with potentially important applications. Catalytic activity was improved by enhancing binding affinity, suggesting the applicability of this procedure to nonenzymatic protein targets as well. Practical applications in these cases may include mutant design of proteins (sometimes receptors) toward, for example, altering specificity against natural ligands (e.g., steroid binding proteins) or increasing affinity for specific ligands (e.g., ligand traps). Our procedure for developing protein mutants with improved binding affinity and altered specificity toward specific ligand(s) consists of (1) design, synthesis, and assay of a congeneric analogue series for systematic probing of the binding site around the targeted ligand(s), (2) development of a 3D-QSAR model from the congeneric series data, (3) selection of mutations based on the QSAR-based 3D profile of binding contributions embedded into the putative binding site, and (4) production and assay of mutants against the targeted ligand(s). Providing successful production of mutant variants and robust enzymatic and/or binding assays, this multistep procedure is in principle applicable to any protein binding site, subject to the availability of experimental structure for the wild-type protein and 3D structural data (experimental or modeled) for the protein-bound ligand core scaffold (the tetrahedral intermediate binding mode in this study). Another important aspect that can affect the applicability of the method is the designed congeneric series of probe analogues, which have to be synthetically feasible, provide chemical space coverage and sampling around the targeted ligand(s), and also lead as much as possible to an unambiguous structural alignment starting from the common core scaffold. The latter aspect is important in obtaining a robust QSAR model and meaningful 3D map of binding contributions with alignment-based methods like MTD-PLS or CoMFA. Suggestions in this direction are small incremental changes between close analogues (as in this study) and/or incorporation of rigid moieties for large substituents (e.g., cyclopentanoyl, cyclohexanoyl, and the 3-fold symmetric dimethylpropionyl included in the series presented here). High flexibility of the targeted ligand (e.g., hexanoyl in this study), as well as structural plasticity of the protein at candidate mutation sites, might however limit the success of this procedure.

In conclusion, besides clear similarities between the acyl-binding pockets of human and porcine Acy1 (Figure 1), especially in the acetyl-accommodating portion, our 3D QSAR analysis points to marked differences between the two enzymes. Porcine Acy1 features a more spacious and continuous pocket at regions more distant from the reaction center, well-suited for the accommodation of extended straight-chain acyl substituents. For hAcy1, however, we predict spatial confinement at a distal site in the pocket, possibly involving Ile177. Using mutational analyses, we confirmed predicted roles of Thr347 and Leu372 in hAcy1 in the steric hindrance of acyl-chain branching at the α- and β-positions, respectively. Our results have potential implications for the use of pAcy1 in biocatalysis and hAcy1 in biomedicine. The T347S mutant of hAcy1 in particular displays greatly improved *N*-benzoylamino acid hydrolyzing activity, demonstrating the potential for engineering of substrate specificity in this enzyme. Further modification may generate a CPG2-like variant of hAcy1 able to hydrolyze MTX and/or applicable in enzyme prodrug activation. Coupling designed series of probe analogues with protein–ligand docking and 3D-QSAR methods like MTD-PLS may also have more general application in the design of proteins with tailored ligand binding affinities and specificities.

SUPPORTING INFORMATION AVAILABLE

MTD hypermolecule occupancy vectors for each acyl group. This material is available free of charge via the Internet at http://pubs.acs.org.

REFERENCES

1. Rawlings, N. D., Morton, F. R., and Barrett, A. J. (2006) MEROPS: The peptidase database. *Nucleic Acids Res. 34*, D270–D272.
2. Rawlings, N. D., and Barrett, A. J. (2004) Introduction: Metallopeptidases and their clans, in *Handbook of Proteolytic Enzymes* (Barrett, A. J., Rawlings, N. D., and Woessner, J. F., Eds.) 2nd ed., pp 231–268, Elsevier, London.
3. Biagini, A., and Puigserver, A. (2001) Sequence analysis of the aminoacylase-1 family. A new proposed signature for metalloexopeptidases. *Comp. Biochem. Physiol., Part B: Biochem. Mol. Biol. 128*, 469–481.
4. Agarwal, R., Burley, S. K., and Swaminathan, S. (2007) Structural Analysis of a Ternary Complex of Allantoate Amidohydrolase from *Escherichia coli* Reveals its Mechanics. *J. Mol. Biol. 368*, 450–463.
5. Todd, C. D., and Polacco, J. C. (2006) AtAAH encodes a protein with allantoate amidohydrolase activity from *Arabidopsis thaliana*. *Planta 223*, 1108–1113.
6. Lundgren, S., Gojkovic, Z., Piskur, J., and Dobritzsch, D. (2003) Yeast β-Alanine Synthase Shares a Structural Scaffold and Origin with Dizinc-dependent Exopeptidases. *J. Biol. Chem. 278*, 51851–51862.
7. Meinnel, T., Schmitt, E., Mechulam, Y., and Blanquet, S. (1992) Structural and biochemical characterization of the *Escherichia coli* argE gene product. *J. Bacteriol. 174*, 2323–2331.
8. Boyen, A., Charlier, D., Charlier, J., Sakanyan, V., Mett, I., and Glansdorff, N. (1992) Acetylornithine deacetylase, succinyldiaminopimelate desuccinylase and carboxypeptidase G2 are evolutionarily related. *Gene 116*, 1–6.
9. Holz, R. C., Bzymek, K. P., and Swierczek, S. I. (2003) Co-catalytic metallopeptidases as pharmaceutical targets. *Curr. Opin. Chem. Biol. 7*, 197–206.
10. Martinez-Rodriguez, S., Clemente-Jimenez, J. M., Rodriguez-Vico, F., and Las Heras-Vazquez, F. J. (2005) Molecular cloning and

biochemical characterization of L-N-carbamoylase from *Sinorhizobium meliloti* CECT4114. *J. Mol. Microbiol. Biotechnol. 9*, 16–25.

11. Ohmachi, T., Narita, M., Kawata, M., Bizen, A., Tamura, Y., and Asada, Y. (2004) A novel N-carbamoyl-L-amino acid amidohydrolase of *Pseudomonas* sp. strain ON-4a: Purification and characterization of N-carbamoyl-L-cysteine amidohydrolase expressed in *Escherichia coli*. *Appl. Microbiol. Biotechnol. 65*, 686–693.

12. Sakanyan, V., Desmarez, L., Legrain, C., Charlier, D., Mett, I., Kochikyan, A., Savchenko, A., Boyen, A., Falmagne, P., and Pierard, A. (1993) Gene cloning, sequence analysis, purification, and characterization of a thermostable aminoacylase from *Bacillus stearothermophilus*. *Appl. Environ. Microbiol. 59*, 3878–3888.

13. Curley, P., van der, D. C., Driessen, A. J., Kok, J., and van Sinderen, D. (2003) Purification and characterisation of a lactococcal aminoacylase. *Arch. Microbiol. 179*, 402–408.

14. Story, S. V., Grunden, A. M., and Adams, M. W. (2001) Characterization of an aminoacylase from the hyperthermophilic archaeon *Pyrococcus furiosus*. *J. Bacteriol. 183*, 4259–4268.

15. Toogood, H. S., Hollingsworth, E. J., Brown, R. C., Taylor, I. N., Taylor, S. J., McCague, R., and Littlechild, J. A. (2002) A thermostable L-aminoacylase from *Thermococcus litoralis*: Cloning, overexpression, characterization, and applications in biotransformations. *Extremophiles 6*, 111–122.

16. Jakob, M., Miller, Y. E., and Röhm, K. H. (1992) Cloning and sequence analyses of cDNAs encoding aminoacylase I from porcine kidney. *Biol. Chem. Hoppe-Seyler 373*, 1227–1231.

17. Cook, R. M., Burke, B. J., Buchhagen, D. L., Minna, J. D., and Miller, Y. E. (1993) Human aminoacylase-1. Cloning, sequence, and expression analysis of a chromosome 3p21 gene inactivated in small cell lung cancer. *J. Biol. Chem. 268*, 17010–17017.

18. Giardina, T., Perrier, J., and Puigserver, A. (2000) The rat kidney acylase I, characterization and molecular cloning. Differences with other acylases I. *Eur. J. Biochem. 267*, 6249–6255.

19. Perrier, J., Durand, A., Giardina, T., and Puigserver, A. (2004) The rat kidney acylase 1. Evidence for a new cDNA form and comparisons with the porcine intestinal enzyme. *Comp. Biochem. Physiol., Part B: Biochem. Mol. Biol. 138*, 277–283.

20. Lin, L. L., Chen, M. H., Chien, H. C. R., Kan, S. C., Chen, C. C., Hu, H. Y., and Hsu, W. H. (2007) Characterization of a bifunctional aminoacylase/carboxypeptidase from radioresistant bacterium *Deinococcus radiodurans* R1. *J. Biotechnol. 128*, 322–334.

21. Ishikawa, K., Ishida, H., Matsui, I., Kawarabayasi, Y., and Kikuchi, H. (2001) Novel Bifunctional Hyperthermostable Carboxypeptidase/Aminoacylase from *Pyrococcus horikoshii* OT3. *Appl. Environ. Microbiol. 67*, 673–679.

22. Taylor, I. N., Brown, R. C., Bycroft, M., King, G., Littlechild, J. A., Lloyd, M. C., Praquin, C., Toogood, H. S., and Taylor, S. J. (2004) Application of thermophilic enzymes in commercial biotransformation processes. *Biochem. Soc. Trans. 32*, 290–292.

23. Hsu, S. K., Lo, H. H., Kao, C. H., Lee, D. S., and Hsu, W. H. (2006) Enantioselective Synthesis of L-Homophenylalanine by Whole Cells of Recombinant *Escherichia coli* Expressing L-Aminoacylase and L-Acylamino Acid Racemase Genes from *Deinococcus radiodurans* BCRC12827. *Biotechnol. Prog. 22*, 1578–1584.

24. Bommarius, A. S. (2002) Hydrolysis of N-acylamino acids, in *Enzyme Catalysis in Organic Synthesis* (Drauz, K., and Waldmann, H., Eds.) 2nd ed., pp 741–760, Wiley-VCH, Weinheim, Germany.

25. Gröger, H., Trauthwein, H., Buchholz, S., Drauz, K., Sacherer, C., Godfrin, S., and Werner, H. (2004) The first aminoacylase-catalyzed enantioselective synthesis of aromatic β-amino acids. *Org. Biomol. Chem. 2*, 1977–1978.

26. Pittelkow, S., Lindner, H., and Röhm, K. H. (1998) Human and porcine aminoacylase I overproduced in a baculovirus expression vector system: Evidence for structural and functional identity with enzymes isolated from kidney. *Protein Expression Purif. 12*, 269–276.

27. Fu, S.-C. J., and Birnbaum, S. M. (1953) The hydrolytic action of acylase I on N-acylamino acids. *J. Am. Chem. Soc. 75*, 918–920.

28. Birnbaum, S. M., Levintov, L., Kingsley, R. B., and Greenstein, J. P. (1952) Specifity of amino acid acylases. *J. Biol. Chem. 194*, 455–470.

29. Wada, I., Handa, M., Imamura, M., Sakiyama, T., Adachi, S., Matsuno, R., and Nakanishi, K. (2002) Enzymatic synthesis of N-acyl-L-amino acids in a glycerol-water system using acylase I from pig kidney. *JAOCS 79*, 41–46.

30. Schmiedeberg, O. (1881) Über Spaltungen und Synthesen im Thierkörper. *Naunyn-Schmiedebergs Arch. Exp. Pathol. Pharmakol. 14*, 379–392.

31. Jones, W. M., Scaloni, A., Bossa, F., Popowicz, A. M., Schneewind, O., and Manning, J. M. (1991) Genetic relationship between acylpeptide hydrolase and acylase, two hydrolytic enzymes with similar binding but different catalytic specificities. *Proc. Natl. Acad. Sci. U.S.A. 88*, 2194–2198.

32. Sass, J. O., Mohr, V., Olbrich, H., Engelke, U., Horvath, J., Fliegauf, M., Loges, N. T., Schweitzer-Krantz, S., Moebus, R., Weiler, P., Kispert, A., Superti-Furga, A., Wevers, R. A., and Omran, H. (2006) Mutations in ACY1, the Gene Encoding Aminoacylase 1, Cause a Novel Inborn Error of Metabolism. *Am. J. Hum. Genet. 78*, 401–409.

33. Van Coster, R. N., Gerlo, E. A., Giardina, T. G., Engelke, U. F., Smet, J. E., De Praeter, C. M., Meersschaut, V. A., De Meirleir, L. J., Seneca, S. H., and Devreese, B. (2005) Aminoacylase I deficiency: A novel inborn error of metabolism. *Biochem. Biophys. Res. Commun. 338*, 1322–1326.

34. Nguyen, K. T., and Pei, D. (2005) Purification and Characterization of Enzymes Involved in the Degradation of Chemotactic N-Formyl Peptides. *Biochemistry 44*, 8514–8522.

35. Ötvös, L., Moravcsik, E., and Mády, G. (1971) Investigation on the mechanism of acylase-I-catalyzed acylamino acid hydrolysis. *Biochem. Biophys. Res. Commun. 44*, 1056–1064.

36. Steele, M., Marcone, M., Gyles, C., Chan, V. L., and Odumeru, J. (2006) Enzymatic activity of *Campylobacter jejuni* hippurate hydrolase. *Protein Eng. Des. Sel. 19*, 17–25.

37. Levy, C. C., and Goldman, P. (1967) The enzymatic hydrolysis of methotrexate and folic acid. *J. Biol. Chem. 242*, 2933–2938.

38. Niculescu-Duvaz, D., Niculescu-Duvaz, I., and Springer, C. J. (2004) Design of prodrugs for suicide gene therapy. *Methods Mol. Med. 90*, 161–202.

39. Schepelmann, S., Spooner, R., Friedlos, F., and Marais, R. (2004) Methods to improve efficacy in suicide gene therapy approaches: Targeting prodrug-activating enzymes carboxypeptidase G2 and nitroreductase to different subcellular compartments, in *Suicide Gene Therapy* (Springer, C. J., Ed.) pp 279–301, Humana Press Inc., Totowa, NJ.

40. Pedley, R. B., Sharma, S. K., Hawkins, R. E., and Chester, K. A. (2004) Antibody-directed enzyme-prodrug therapy, in *Suicide Gene Therapy* (Springer, C. J., Ed.) pp491–514, Humana Press Inc., Totowa, NJ.

41. Rowsell, S., Pauptit, R. A., Tucker, A. D., Melton, R. G., Blow, D. M., and Brick, P. (1997) Crystal structure of carboxypeptidase G2, a bacterial enzyme with applications in cancer therapy. *Structure 5*, 337–347.

42. Hakansson, K., and Miller, C. G. (2002) Structure of peptidase T from *Salmonella typhimurium*. *Eur. J. Biochem. 269*, 443–450.

43. Badger, J., Sauder, J. M., Adams, J. M., Antonysamy, S., Bain, K., Bergseid, M. G., Buchanan, S. G., Buchanan, M. D., Batiyenko, Y., Christopher, J. A., Emtage, S., Eroshkina, A., Feil, I., Furlong, E. B., Gajiwala, K. S., Gao, X., He, D., Hendle, J., Huber, A., Hoda, K., Kearins, P., Kissinger, C., Laubert, B., Lewis, H. A., Lin, J., Loomis, K., Lorimer, D., Louie, G., Maletic, M., Marsh, C. D., Miller, I., Molinari, J., Muller-Dieckmann, H. J., Newman, J. M., Noland, B. W., Pagarigan, B., Park, F., Peat, T. S., Post, K. W., Radojicic, S., Ramos, A., Romero, R., Rutter, M. E., Sanderson, W. E., Schwinn, K. D., Tresser, J., Winhoven, J., Wright, T. A., Wu, L., Xu, J., and Harris, T. J. (2005) Structural analysis of a set of proteins resulting from a bacterial genomics project. *Proteins 60*, 787–796.

44. Shi, D., Yu, X., Roth, L., Tuchman, M., and Allewell, N. M. (2007) Structure of a novel N-acetyl-L-citrulline deacetylase from *Xanthomonas campestris*. *Biophys. Chem. 126*, 86–93.

45. Jozic, D., Bourenkow, G., Bartunik, H., Scholze, H., Dive, V., Henrich, B., Huber, R., Bode, W., and Maskos, K. (2002) Crystal Structure of the Dinuclear Zinc Aminopeptidase PepV from *Lactobacillus delbrueckii* Unravels Its Preference for Dipeptides. *Structure 10*, 1097–1106.

46. Lundgren, S., Andersen, B., Piskur, J., and Dobritzsch, D. (2007) Crystal structures of yeast β-alanine synthase complexes reveal the mode of substrate binding and large-scale domain closure movements. *J. Biol. Chem. 282*, 36037–36047.

47. Bzymek, K. P., and Holz, R. C. (2004) The Catalytic Role of Glutamate 151 in the Leucine Aminopeptidase from *Aeromonas proteolytica*. *J. Biol. Chem. 279*, 31018–31025.

48. Wouters, M. A., and Husain, A. (2001) Changes in zinc ligation promote remodeling of the active site in the zinc hydrolase superfamily. *J. Mol. Biol. 314*, 1191–1207.

49. Lindner, H. A., Lunin, V. V., Alary, A., Hecker, R., Cygler, M., and Ménard, R. (2003) Essential roles of zinc ligation and enzyme dimerization for catalysis in the aminoacylase-1/M20 family. *J. Biol. Chem. 278*, 44496–44504.

50. Lindner, H. A., Alary, A., Boju, L. I., Sulea, T., and Ménard, R. (2005) Roles of Dimerization Domain Residues in Binding and Catalysis by Aminoacylase-1. *Biochemistry 44*, 15645–15651.

51. Martinez-Rodriguez, S., Andujar-Sanchez, M., Clemente Jimenez, J. M., Jara-Perez, V., Rodriguez-Vico, F., and Heras-Vazquez, F. J. L. (2006) Thermodynamic and mutational studies of L-N-carbamoylase from *Sinorhizobium meliloti* CECT 4114 catalytic centre. *Biochimie 88*, 837–847.

52. Bradford, M. M. (1976) A rapid and sensitive method for the quantitation of microgram quantities of protein utilizing the principle of protein-dye binding. *Anal. Biochem. 72*, 248–254.

53. Lindner, H., Berens, W., Kraus, I., and Röhm, K. H. (2000) Mutational analysis of two PWW sequence motifs in human aminoacylase 1. *Biol. Chem. 381*, 1055–1061.

54. Kurunczi, L., Seclaman, E., Oprea, T. I., Crisan, L., and Simon, Z. (2005) MTD-PLS: A PLS Variant of the Minimal Topologic Difference Method. III. Mapping Interactions between Estradiol Derivatives and the Alpha Estrogenic Receptor. *J. Chem. Inf. Model. 45*, 1275–1281.

55. Kurunczi, L., Olah, M., Oprea, T. I., Bologa, C., and Simon, Z. (2002) MTD-PLS: A PLS-Based Variant of the MTD Method. 2. Mapping Ligand-Receptor Interactions. Enzymatic Acetic Acid Esters Hydrolysis. *J. Chem. Inf. Model. 42*, 841–846.

56. Oprea, T. I., Kurunczi, L., Olah, M., and Simon, Z. (2001) MTD-PLS: A PLS-Based Variant of the MTD Method. A 3D-QSAR Analysis of Receptor Affinities for a Series of Halogenated Dibenzoxin and Biphenyl Derivatives. *SAR QSAR Environ. Res. 12*, 75–92.

57. Pearlman, R. S. (1987) Rapid Generation of High Quality Approximate 3D Molecular Structures. *Chem. Des. Auto. News 2*, 1–7.

58. Simon, Z., Chiriac, A., Holban, S., Cubotariu, D., and Mihalas, G. I. (1984) *Minimum Steric Difference. The MTD Method for QSAR Studies*, Research Studies Press, Letchworth, U.K.

59. Ciubotariu, D., Deretey, E., Oprea, T. I., Sulea, T., Simon, Z., Kurunczi, L., and Chiriac, A. (1993) Multiconformational minimal steric difference. Structure-acetylcholinesterase hydrolysis rates relations for acetic acid esters. *Quant. Struct.-Act. Relat. 12*, 367–372.

60. Oprea, T. I., Ciubotariu, D., Sulea, T., and Simon, Z. (1993) Comparison of the minimal steric difference (MTD) and comparative molecular field analysis (CoMFA) methods for analysis of binding of steroids to carrier proteins. *Quant. Struct.-Act. Relat. 12*, 21–26.

61. Simon, Z. (1993) MTD and Hyperstructure Approaches, in *3D QSAR in Chemistry* (Kubinyi, H., Ed.) pp 307–309, ESCOM, Leiden, The Netherlands.

62. Greco, G., Novellino, E., and Martin, Y. C. (1997) Approaches to Three-Dimensional Quantitative Structure-Activity Relationships, in *Reviews in Computational Chemistry* (Lipkowitz, K. B., and Boyd, D., Eds.) pp 183–240, Wiley-VCH, New York.

63. Oprea, T. I., and Waller, C. L. (1997) Theoretical and Practical Aspects of Three-Dimensional Quantitative Structure-Activity Relationships, in *Reviews in Computational Chemistry* (Lipkowitz, K. B., and Boyd, D., Eds.) pp 127–182, Wiley-VCH, New York.

64. Wold, S., Ruhe, A., Wold, H., and Dunn, W. J. The Collinearity Problem in Linear Regression. The Partial Least Squares (PLS) Approach to Generalized Inverses. *SIAM J. Sci. Stat. Comput. 5*, 735–743.

65. Höskuldsson, A. (1988) PLS regression methods. *J. Chemom. 2*, 211–228.

66. Wold, S., Sjöström, M., and Eriksson, L. (1999) PLS in Chemistry, in *The Encyclopedia of Computational Chemistry* (Schleyer, P. V. R., Allinger, N. L., Clark, T., Gasteiger, J., Kollman, P. A., Schaefer, H. F., and Schreiner, P. R., Eds.) pp 2006–2020, John Wiley & Sons, Chichester, U.K.

67. Cramer, R. D., Patterson, D. E., and Bunce, J. D. (1988) Comparative molecular field analysis (CoMFA). 1. Effect of shape on binding of steroids to carrier proteins. *J. Am. Chem. Soc. 110*, 5959–5967.

68. Ferrara, P., Gohlke, H., Price, D. J., Klebe, G., and Brooks, C. L. (2004) Assessing scoring functions for protein-ligand Interactions. *J. Med. Chem. 47*, 3032–3047.

69. Wang, R., Lu, Y., Fang, X., and Wang, S. (2004) An extensive test of 14 scoring functions using the PDBbind refined set of 800 protein-ligand complexes. *J. Chem. Inf. Comput. Sci. 44*, 2114–2125.

70. Warren, G. L., Andrews, C. W., Capelli, A. M., Clarke, B., LaLonde, J., Lambert, M. H., Lindvall, M., Nevins, N., Semus, S. F., Senger, S., Tedesco, G., Wall, I. D., Woolven, J. M., Peishoff, C. E., and Head, M. S. (2006) A critical assessment of docking programs and scoring functions. *J. Med. Chem. 49*, 5912–5931.

71. Rajamani, R., and Good, A. C. (2007) Ranking poses in structure-based lead discovery and optimization: Current trends in scoring function development. *Curr. Opin. Drug Discovery Dev. 10*, 308–315.

72. Huang, N., and Jacobson, M. P. (2007) Physics-based methods for studying protein-ligand interactions. *Curr. Opin. Drug Discovery Dev. 10*, 325–331.

73. Kroemer, R. T. (2007) Structure-based drug design: Docking and scoring. *Curr. Protein Pept. Sci. 8*, 312–328.

74. Coupez, B., and Lewis, R. A. (2006) Docking and scoring: Theoretically easy, practically impossible? *Curr. Med. Chem. 13*, 2995–3003.

75. Sheinerman, F. B., and Honig, B. (2002) On the role of electrostatic interactions in the design of protein-protein interfaces. *J. Mol. Biol. 318*, 161–177.

76. Gohlke, H., Kiel, C., and Case, D. A. (2003) Insights into protein-protein binding by binding free energy calculation and free energy decomposition for the Ras-Raf and Ras-RalGDS complexes. *J. Mol. Biol. 330*, 891–913.

77. Velec, H. F. G., Gohlke, H., and Klebe, G. (2005) DrugScoreCSD-knowledge-based scoring function derived from small molecule crystal data with superior recognition rate of near-native ligand poses and better affinity prediction. *J. Med. Chem. 48*, 6296–6303.

78. Di Fenza, A., Heine, A., Koert, U., and Klebe, G. (2007) Understanding binding selectivity toward trypsin and factor Xa: The role of aromatic interactions. *ChemMedChem 2*, 297–308.